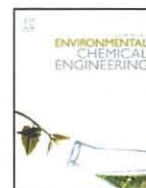Contents lists available at ScienceDirect

Journal of Environmental Chemical Engineering

journal homepage: www.elsevier.com/locate/jece

Adsorption of two cationic textile dyes from water with modified nanoclay: A comparative study by using central composite design

CrossMark

Aydin Hassani[a], Alireza Khataee[b,*], Semra Karaca[a,**], Melike Karaca[a], Murat Kıranşan[a]

[a] Department of Chemistry, Faculty of Science, Atatürk University, 25240 Erzurum, Turkey
[b] Research Laboratory of Advanced Water and Wastewater Treatment Processes, Department of Applied Chemistry, Faculty of Chemistry, University of Tabriz, 51666-16471 Tabriz, Iran

ARTICLE INFO

ABSTRACT

Comparative removal of two cationic dyes, Basic Green 4 (BG4) and Basic Yellow 28 (BY28), by chemically modified nanoclay was optimized using the central composite design. The chemically modified nanoclay was characterized by SEM, EDX, FTIR, XRD and BET techniques. The average crystal size of nanoclay was about 16.5 nm. The accuracy of the model and regression coefficients was appraised by employing the analysis of variance (ANOVA). The results revealed a good agreement between the predicted values, as obtained by the model, and the experimental values for both BG4 ($R^2 = 0.960$) and BY28 ($R^2 = 0.927$). The optimum conditions proposed by central composite design to reach the maximum dye removal through adsorption process. Under the optimum conditions, the removal efficiency of BG4 and BY28 were 82.35% and 98.78%, respectively. For BG4 and BY28, the pH of solution and adsorbent dosage were found to be the key factors that controlled dye adsorption, respectively.

© 2015 Elsevier Ltd. All rights reserved.

1. Introduction

The rapid growth in the use of synthetic dyes in the textile industry has led to a significant increase in environmental pollution. Many of these dyes are toxic and therefore, should be removed from wastewater before being discharged into water resources in order to protect the living organisms [1]. Therefore, the purification of colored wastewater has received much attention in recent years [2,3]. In addition, it should be noted that the presence of organic dyes in water bodies can act against light penetration, thereby hindering photosynthesis [4–6]. Various treatment technologies are employed for the removal of organic dyes from aqueous environments. These are such as coagulation/flocculation [7,8], membrane [9], chemical oxidation [10–13] and biological processes [14–16]. However, these methods have some problems such as plenty waste sludge and high capital cost [17]. Based on the related literature on wastewater treatment, adsorption process can be a promising and efficient method to diminish colored wastewater due to its low cost, insensitivity to toxic substances, simplicity, ease of operation and no sludge formation [18–22]. Nevertheless, it should be noted that in the adsorption process, the most widely used adsorbent is activated

carbon due to its high adsorption capacity, large surface area and porous character [23,24]. The problem is that commercial activated carbon needs relatively high capital cost regeneration [16,25]. Therefore, it is proposed to increase new adsorbents for the decolorization of aqueous solutions. Natural clays have received much attention because they are environmentally friendly, cheap, abundant and ion exchangeable adsorbents [18,26–28]. Montmorillonite, as one of the most widely used adsorbents, has been used for the removal of contaminants from water because it is available, relatively cheap, easily extracted, non-toxic, and mechanically and chemically stable [4,18,29,30]. However, it should be noted that for the removal of target pollutants from the aqueous media, the application of pristine montmorillonite is quite limited. To tackle this problem, one of the most widely used methods is the use of the modified montmorillonite with a suitable chemical agent [18]. Recently, the surface modification of clays by using surfactants or inorganic coatings has been employed to improve their adsorption properties for some organic contaminants [31–33]. In this regard, the organosilane modification of naturally occurring adsorbents for adsorption is very important. On the other hand, it has been shown that expanded pores with various reactive such as alkanes and amines have better adsorption properties for azo dyes. This is due to the interaction possibility provided with large pores between specific functional groups on the modified clay surface and azo dyes [34,35]. The main purpose of the present study modified nanoclay with octadecylamine and aminopropyltriethoxysilane was

---

* Corresponding author. Fax: +98 41 33340191.
** Corresponding author. Fax: +90 442 2360948.
   E-mail addresses: a_khataee@tabrizu.ac.ir, ar_khataee@yahoo.com (A. Khataee), skaraca@atauni.edu.tr, semra_karaca@yahoo.com (S. Karaca).

used for the adsorption of two cationic dyes, C.I. Basic Green 4 (BG4) and C.I. Basic Yellow 28 (BY28), in the aqueous phase. The nanoclay was characterized by SEM, EDX, FTIR, XRD and BET techniques. To further probe the effect of various operational parameters, including the initial dye concentration, contact time, the adsorbent dosage and the pH of the solution, on the adsorption of BG4 and BY28 via the adsorption technique, response surface methodology (RSM) based on central composite design (CCD) was employed. RSM was selected as an effective statistical and mathematical approach in order to recognize the efficiency of an experimental system [36,37]. Various parameters were simultaneously appraised using RSM with a minimum number of experiments. Therefore, a study conducted by RSM can reduce the cost, decrease process variability and need less time in comparison to the conventional one-factor-at-a-time statistical strategy [38–40].

2. Experimental

2.1. Materials

The adsorbent studied in the present work was montmorillonite nanoclay chemically modified with 15–35 wt.% octadecylamine and 0.5–5 wt.% aminopropyltriethoxysilane (Sigma-Aldrich Co.). All reagents used were provided by Merck Co. (Germany), with analytical grades, and used without further purification. The two cationic textile dyes, Basic Green 4 (BG4) and Basic Yellow 28 (BY28), were supplied by Shimi Boyakhsaz Company, Iran, and used as received. The characteristics of supplied dyes can be seen in Table 1.

2.2. Adsorption studies

In the evaluation of the chemically modified nanoclay adsorbent for the removal of the organic dyes from aqueous solutions, all experiments were conducted by employing the batch adsorption procedure. For adsorption studies, initial dye concentration, contact time, adsorbent dosage and the pH of the solutions were as 20–40 mg/L, 10–60 min, 0.25–0.65 g/L and 2–10, respectively. The pH of solutions was adjusted using 0.1 M HCl or 0.1 M NaOH solution and monitored by a digital pH-meter (model CG 840, Germany). The mixture was kept under agitation at 150 rpm in a temperature controlled shaker (Julabo SW22, Germany). At the end of each experimental run, the sample was withdrawn and immediately centrifuged at 6000 rpm for 10 min in order to determine the residual concentration of BG4 and BY28 dyes via a Varian Cary 100 UV–visible spectrophotometer (Australia); this was done by monitoring the absorbance change at 618 and 439 nm, respectively. The dye removal efficiency was calculated using Eq. (1):

$$\text{Removal efficiency}(\%) = \frac{(C_0 - C_t)}{C_0} \times 100 \tag{1}$$

where C_0 (mg/L) and C_t (mg/L) are the concentrations of the dyes at the beginning and time t, respectively. The amount of adsorbed dye (q) as mg/g was calculated via Eq. (2):

$$q = \frac{(C_0 - C_e) \times V}{M} \tag{2}$$

where C_0 (mg/L) and C_e (mg/L) are the initial and equilibrium concentrations of the dye, respectively. Moreover, V (L) is the volume of the solution and M (g) is the mass of the adsorbent.

2.3. Characterizations

Brunauer–Emmett–Teller (BET) analysis was conducted to determine the specific surface area of the adsorbent by means of N_2 adsorption–desorption isotherm, which was measured at

Table 1
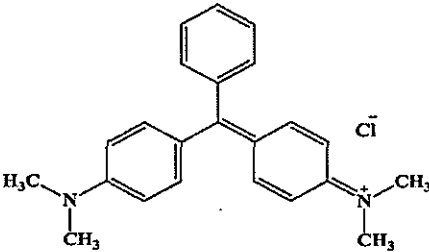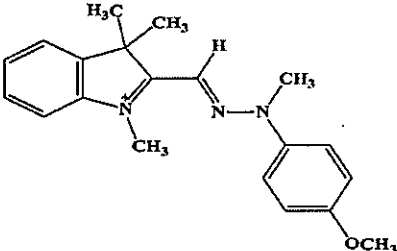Characteristics of C.I. Basic Green 4 and C.I. Basic Yellow 28.

Color index name	Chemical structure	Molecular formula	M_w (g/mol)	λ_{max} (nm)	Class
Basic Green 4 (BG4)		$C_{23}H_{25}ClN_2$	364.91	618	Triarylmethane
Basic Yellow 28 (BY28)		$C_{21}H_{27}N_3O_5S$	433.52	439	Methine

Table 2
Process variables and their experimental levels.

Factor	Ranges and levels				
	-2	-1	0	+1	+2
[Dye]$_0$ (mg/L) (X_1)	20	25	30	35	40
Contact time (min) (X_2)	10	22.5	35	47.5	60
Adsorbent dosage (g/L) (X_3)	0.25	0.35	0.45	0.55	0.65
pH (X_4)	2	4	6	8	10

77 K in the relative pressure range, from 0.05 to 0.4 (Belsorp mini II Bel, Japan). Barret–Joyner–Halender (BJH) method was used to obtain the pore size distribution [41]. The sample was degassed at 100 °C for 15 h in the degas port of the analyzer prior to measurement. A Philips XL 30 SFEG model (the Netherlands) scanning electron microscope (SEM) was employed to characterize the surface morphology of chemically modified nanoclay. On the other hand, energy-dispersive X-ray spectroscopic (EDX) study was launched to characterize the chemical composition of the adsorbent. X-ray diffraction (XRD, STOE D-64295, Germany) of nanoclay studies was performed using Cu-Kα X-radiation (λ = 0.15406 nm). The Fourier transform infrared (FTIR) spectra of as-prepared samples, before and after measuring the adsorption of the dyes, were obtained in the wavenumber range of 400–4000 cm^{-1} using a Perkin Elmer spectrometer (Model: 1600, USA). The zeta potential of the modified nanoclay/water suspension was measured using Zeta-Meter 3.0+, Inc., Staunton, VA, USA.

2.4. Experimental design

To determine the optimal conditions for the main parameters, a central composite design (CCD) was applied. For the adsorption process, significant variables, such as the initial dye concentration, contact time, the adsorbent dosage and the pH of the solution, were regarded as the independent variables and designated as X_1–X_4, respectively. The dye concentration (X_1) range of 20–40 mg/L, the contact time (X_2) range of 10–60 min, the adsorbent dosage (X_3) of 0.25–0.65 g/L and the solution pH (X_4) range of 2–10 were chosen as given in Table 2. According to the CCD model, the number of experimental runs was calculated using Eq. (3):

$$N = 2^k + 2k + x_0 \tag{3}$$

where N, k and x_0 represent the number of experimental runs, the number of parameters and the number of central points, respectively [4,27]. Therefore, the total number of experimental runs was obtained be 31 ($k=4$, $x_0=7$). The parameters (X_i) were

coded as x_i via Eq. (4):

$$x_i = \frac{(X_i - X_0)}{\delta X} \tag{4}$$

where X_0 and δX are the values of X_i at the center point and step change, respectively [4,18].

The second-order polynomial response equation was used to probe the interaction between the dependent and independent variables. A second-order polynomial approximation of experimental results expression was also used to relate the dependent (removal efficiency (%)) and independent variables as shown by Eq. (5).

$$Y = \beta_0 + \sum_{i=1}^{k} \beta_i x_i + \sum_{i=1}^{k} \beta_{ii} x_i^2 + \sum_{i=1}^{k} \sum_{i \neq j=1}^{k} \beta_{ij} x_{i,j} + \varepsilon \tag{5}$$

where Y is the response, β_0 is the constant, β_i is the linear coefficient, β_{ii} is the quadratic coefficient, β_{ij} is the interaction coefficient, x_i is the coded variable level, k is the number of independent variables and ε is the residual term [37,42]. The least square method was used to calculate the model coefficients through Eq. (5) using Design-Expert package (version 7.0.0). To evaluate the statistical significance, ANOVA analysis (R^2, adjusted R^2, F-test and t-test), normal plots and residuals analysis were employed. The significance of the regression coefficients was appraised by the F and Student's t tests at the confidence level of 95%.

3. Results and discussion

3.1. Characterization of modified nanoclay

X-ray diffraction (XRD) pattern of chemically modified nanoclay can be seen in Fig. 1. From the peak positions of the XRD pattern, the basal spacing of chemically modified nanoclay was obtained. The chemically modified nanoclay showed the characteristic peak of the montmorillonite at $2\theta = 8.04°$, which corresponded to the interlayer distance (d_{001}) of 1.09 nm. Moreover, the montmorillonite represented the diffraction peak at 2θ of 8.04°, 19.83°, 34.86°, 53.91° and 61.77° and the quartz at 2θ of 20.8° and 26.6°. These made the dominant phase of the chemically modified nanoclay, thereby indicating the XRD pattern of the prepared nanoclay [43,44]. The average crystal size of the chemically
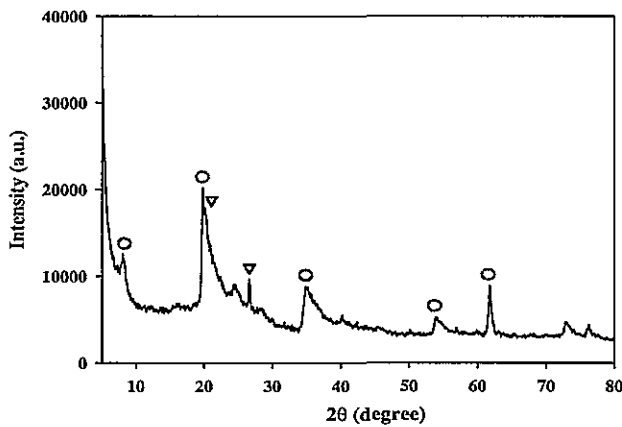

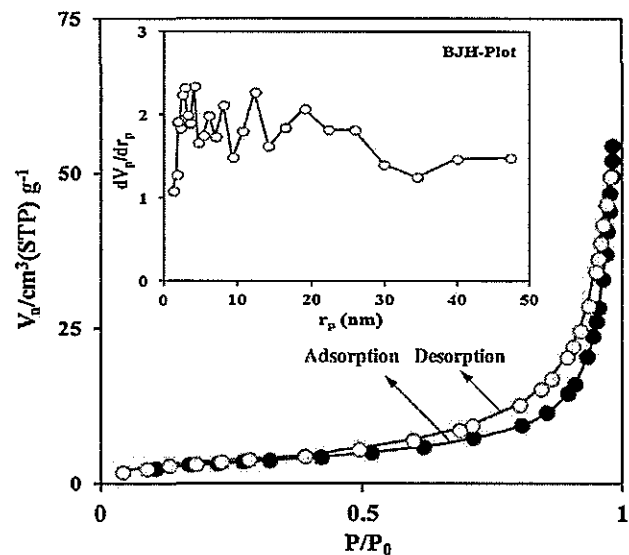**Fig. 1.** XRD pattern of chemically modified nanoclay. (◯) Montmorillonite, (▽) Quartz.

Fig. 2. N$_2$ adsorption–desorption isotherm of modified nanoclay and the inset showing BJH pore size distribution plot.
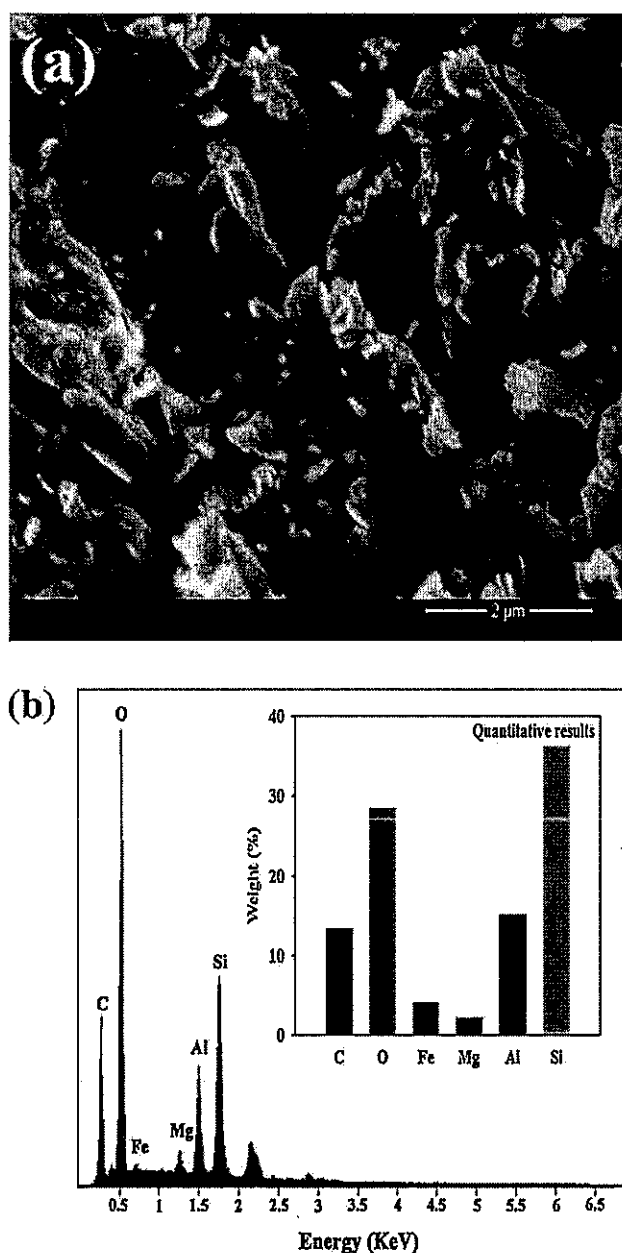
Fig. 3. Scanning electron microscopy image of modified nanoclay surface (a) and EDX spectrum with inset showing weight percent of elements (b).

modified nanoclay was quantitatively assessed using Debye–Scherrer equation $d = (k\lambda/\beta\cos\theta)$. In this equation, d is the crystal size (nm), k is the Debye–Scherrer constant (0.9), λ is the X-ray wavelength (0.15406 nm), β is the width of the peak with the maximum intensity in half height and θ is the diffraction angle. The average crystal size for the interlayer spacing of chemically modified nanoclay is 16.5 nm ($2\theta = 8.04°$). The N_2 adsorption–desorption isotherm and pore size distribution for chemically modified nanoclay used as the adsorbent can be seen in Fig. 2. The BET surface area of the chemically modified nanoclay was calculated from the N_2 isotherm at 77 K. As can be seen, the adsorbent particles had an isotherm type IV because hysteresis occurred during the desorption branches, according to the IUPAC classification. This showed that the lower (adsorption) branch represented measurements by the progressive addition of gas

molecules to the system. Also, the upper (desorption) branch characteristic of the mesoporous solids was due to the gas (nitrogen) condensation by the progressive withdrawal [45–47]. The isotherm of the chemically modified clay (Fig. 2) presented a type-H3 hysteresis loop (no limiting adsorption was observed at high P/P_0). This could be ascribed to the aggregates (loose assemblages) of plate-like particles forming slit like pores with nonuniform size and/or shape and wide mouths [46,47]. The other possibility could be capillary condensation in mesopores [48]. Isotherm graph showed that the hysteresis loop appeared at high pressure range (nearly $P/P_0 > 0.5$) while adsorption and desorption lines were overlapped completely in the low relative pressure range, thereby indicating the presence of the ink-bottle type of pores [49,50], such ink-bottle pores, which had a large pore diameter since hysteresis occurred at high relative pressures (P/P_0) [50]. The extremely lower amounts of nitrogen adsorbed at low relative pressures revealed the presence of predominant meso-pores in the adsorbent structure. This was because the adsorption capacity in microporous solids was higher than that in the mesoporous solids. Moreover, the enhanced absorption in a high relative pressure (P/P_0) range (approaching 1.0) confirmed the existence of larger mesopores [50]. Pore size distributions, as calculated by the BJH method, are shown in the inset of Fig. 2. The BET surface area and monolayer adsorption capacity of chemically modified clay were found to be 11.478 m^2/g and 2.637 cm^3/g, respectively. Moreover, the total pore volume and the mean pore diameter were obtained to be 8.4267×10^{-2} cm^3/g and 29.368 nm, respectively. The BET surface area and the total pore volume of the adsorbent demonstrated the non-uniform textural and the predominantly mesoporous structure of the modified clay sample (see Fig. 2). For the characterization of the surface morphology of the modified nanoclay, the SEM micrograph was prepared as shown in Fig. 3a. As shown, the adsorbent exhibited well distinguishable particles, a heterogeneous porous structure and a rough surface. It could be understood from the porous structure that the dye molecules were more likely to be trapped and adsorbed on to the surface of the adsorbent. Furthermore, EDX
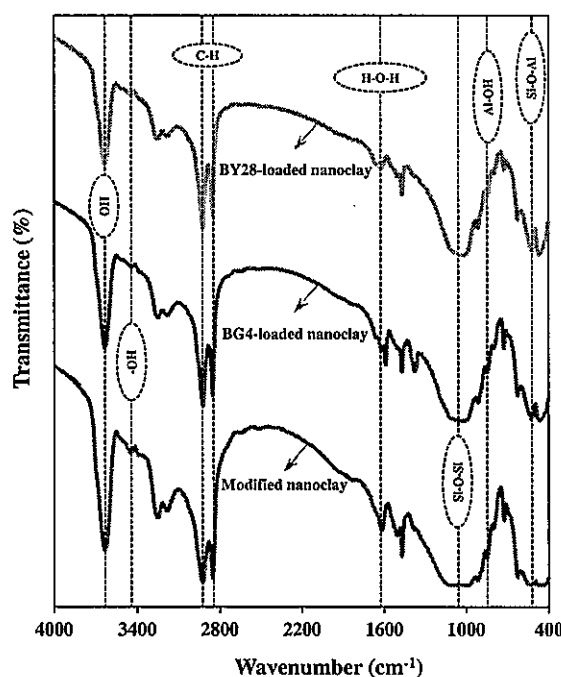

Fig. 4. FTIR spectrum of modified nanoclay before and after the adsorption of BG4 and BY28 at optimum conditions.

Table 3
The 4-factor central composite design matrix and the value of the response function (RE (%)).

Run	[Dye]$_0$ (mg/L)	Contact time (min)	Adsorbent dosage (g/L)	pH	Removal efficiency (%) BG4 Exp.	Pred.	BY28 Exp.	Pred.
1	35	47.5	0.35	4	44.58	46.85	75.66	80.36
2	25	47.5	0.55	8	68.95	68.88	99.94	100.00
3	30	35.0	0.45	6	63.39	63.94	88.67	89.55
4	30	60.0	0.45	6	66.58	66.80	84.37	79.04
5	30	35.0	0.45	6	63.16	63.94	88.82	89.55
6	35	22.5	0.35	4	35.12	36.27	78.91	75.44
7	30	35.0	0.45	6	63.69	63.94	88.68	89.55
8	30	35.0	0.45	2	56.61	50.33	98.88	94.46
9	25	22.5	0.35	4	35.90	39.34	64.85	70.15
10	30	35.0	0.45	6	63.93	63.94	90.48	89.55
11	30	35.0	0.25	6	44.91	44.43	71.85	67.39
12	25	47.5	0.55	4	63.79	65.26	94.69	96.13
13	30	35.0	0.45	10	76.18	79.32	97.14	97.75
14	35	47.5	0.55	8	77.72	76.53	93.59	91.82
15	25	47.5	0.35	4	49.15	49.25	72.73	75.07
16	35	47.5	0.35	8	72.96	70.44	77.05	80.47
17	25	22.5	0.35	8	62.83	61.50	76.01	75.02
18	30	10.0	0.45	6	55.56	52.21	61.51	63.03
19	30	35.0	0.65	6	73.29	70.63	97.34	97.99
20	40	35.0	0.45	6	65.10	64.09	85.76	83.48
21	35	22.5	0.35	8	60.87	61.65	69.10	71.19
22	20	35.0	0.45	6	61.64	59.51	91.57	90.05
23	35	47.5	0.55	4	67.47	69.69	92.12	93.39
24	30	35.0	0.45	6	64.35	63.94	90.23	89.55
25	25	22.5	0.55	8	64.88	64.86	93.77	92.60
26	30	35.0	0.45	6	64.68	63.94	90.59	89.55
27	35	22.5	0.55	8	71.05	71.84	82.80	80.73
28	35	22.5	0.55	4	61.36	63.20	82.46	86.66
29	25	47.5	0.35	8	69.20	69.61	84.96	84.29
30	30	35.0	0.45	6	64.38	63.94	89.38	89.55
31	25	22.5	0.55	4	56.05	59.45	92.56	89.41

measurement of chemically modified nanoclay was carried out to find out the distribution of elements on the sample surface (Fig. 3b). Based on the EDX micrograph, the major portion of the chemically modified nanoclay was found to consist of Si and O compounds, which were suitable for the adsorption of various organic pollutants such as a dye from an aqueous solution. The weight percentage (wt.%) of Si, O, Al, C, Fe and Mg compounds within the adsorbent was 36.26, 28.52, 15.27, 13.43, 4.23 and 2.30%, respectively. FTIR spectra of modified nanoclay samples, before and after the adsorption of BG4 and BY28, were recorded in a wavenumber range between 400 and 4000 cm^{-1}, as shown in Fig. 4. In order to determine the FTIR spectra, the absorption peaks were compared with the standard patterns. The FTIR spectrum of modified clay sample (Fig. 4) showed the characteristic bands; particularly, the bands at 3634 and 3443 cm^{-1} were attributable to the stretching vibrations of the structural and symmetric —OH groups of interlayer water molecule and their frequencies were changed after the adsorption, becoming 3631 and 3442 cm^{-1} for BG4 and 3633 and 3441 cm^{-1} for BY28. This indicated the hydrogen bonds between dyes and the modified clay surface. The bands corresponded to C—H stretching at 2923 and 2852 cm^{-1} and the hydroxyl vibration at 1616 cm^{-1}. After adsorption, the shift was observed in the peaks at 2923 and 2852 cm^{-1} to 2921 and 2851 cm^{-1} for BG4 and 2920 and 2850 cm^{-1} for BY28, thereby reflecting the important effect of CH$_3$, CH$_2$ and CH groups on binding the same dyes onto the modified clay surface. The decrease in the frequency of H—O—H bending vibrations at 1622 cm^{-1} for the pure modified clay confirmed the results of forming H-bonds [51]. The frequency of this band was decreased from 1622 cm^{-1} to 1618 cm^{-1} and 1614 cm^{-1} for BG4 and BY28, respectively (see Fig. 4). Most peaks in the region 1100–400 cm^{-1} could be assigned

to the clay minerals and silicon containing groups [52]. A strong peak that appeared at 1030 cm^{-1} indicated the presence of siloxan (Si—O—Si) bond [52,53]. The band at 800 cm^{-1} was attributed to the vibration of quartz [54]. The FTIR peaks from the modified clay were observed as a broad peak in the range 1162–974 cm^{-1}, which corresponded to the stretching and bending vibrations of Si—O—Al, Si—O— Si and Al—OH—Al, Al—OH—Mg groups. They also became remarkably narrow in the spectra of the pure and dye loaded adsorbent [52,53]. This narrow band was observed in the range of 1114–988 cm^{-1} for BG4 and 1119–997 cm^{-1} for BY28, probably due to the intercalation of dye molecules [53].

3.2. CCD model analysis

To optimize the removal of BG4 and BY28 by adsorption process, a four variable central composite design (CCD) was employed. The individual and interactive effects of independent variables, which included the initial dye concentration, contact time, the adsorbent dosage and the pH of the solution, on the removal efficiency (as response) were investigated using CCD approach. The experimental and predicted removal efficiency (%) for both BG4 and BY28 dyes can be seen in Table 3. Eqs. (6) and (7) indicate the relationship between the response and independent variables for the dyes:

$$Y(BG4) = 63.9445 + 1.1458X_1 + 3.6488X_2 + 6.5513X_3 + 7.2494X_4$$
$$-0.5355X_1^2 - 1.1093X_2^2 - 1.6024X_3^2 + 0.2215X_4^2$$
$$+0.1689X_1X_2 + 1.7056X_1X_3 + 0.8065X_1X_4$$
$$-1.0232X_2X_3 - 0.4478X_2X_4 - 4.1853X_3X_4 \qquad (6)$$

Table 4
Analysis of variance (ANOVA) for response surface quadratic models.

Source	Degree of freedom	BG4			BY28		
		Sum of squares	F-value	P-value	Sum of squares	F-value	P-value
Model	14	3108.69	28.12	0.000	2848.32	14.66	0.000
Residuals	16	126.33			222.12		
Total	30	3235.02			3070.44		

BG4: $R^2 = 0.960$. Adjusted $R^2 = 0.926$.
BY28: $R^2 = 0.927$. Adjusted $R^2 = 0.864$.

$$Y(BY28) = 89.5526 - 1.6422X_1 + 4.0007X_2 + 7.6507X_3$$
$$+0.8237X_4 - 0.6951X_1^2 - 4.6280X_2^2 - 1.7140X_3^2$$
$$+1.6394X_4^2 + 0.0007X_1X_2 - 2.0096X_1X_3 - 2.2784X_1X_4$$
$$+0.4508X_2X_3 + 1.0886X_2X_4 - 0.4197X_3X_4 \qquad (7)$$

The statistical significance of the CCD model was assessed using the analysis of variance (ANOVA) [18,42]. The results of the ANOVA have been summarized in Table 4. It was revealed that the applied model could be successfully used for navigating the design space defined by CCD. According to the data brought in Table 4, the high values of correlation coefficients ($R^2 = 0.960$ for BG4 and $R^2 = 0.927$ for BY28) between the predicted and experimental removal efficiency (%) were obtained. This indicated that the applied model could be reliable for predicting the removal efficiency (%). The plots of predicted removal efficiency (%) versus experimental removal efficiency (%) for both BG4 and BY28 have been depicted in Fig. 5. There was a good agreement between the predicted and experimental removal efficiency (%). In the case of BG4, the obtained value of 0.960 showed that 96.0% of the variations for the removal efficiency (%) could be accounted for by the model and the model could not explain only 4.0% of the variations. In the case of BY28, the obtained value of 0.927 revealed that 92.7% of the variations were accounted for by the model and the model was unable to explain only 7.3% of the variations. Furthermore, the value of adjusted R^2 was in accordance with the value of R^2 with regard to the sample size and the number of variables and statistical terms were based on the degrees of freedom [55,56]. It should be noted that in a system with various independent variables, adjusted R^2 is more appropriate for evaluating the goodness of applied model. In our study, the adjusted R^2 for BG4 (0.926) and the adjusted R^2 for BY28 (0.864)
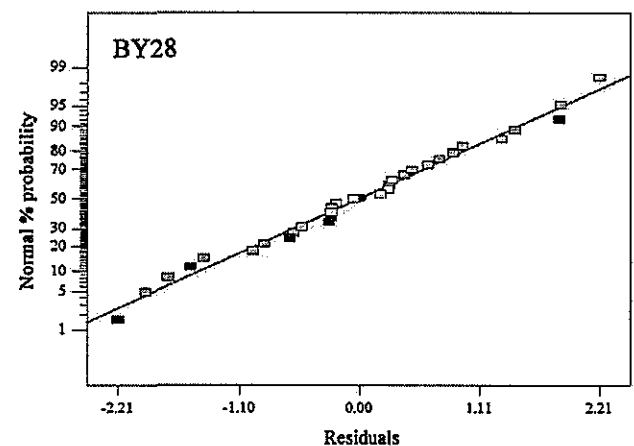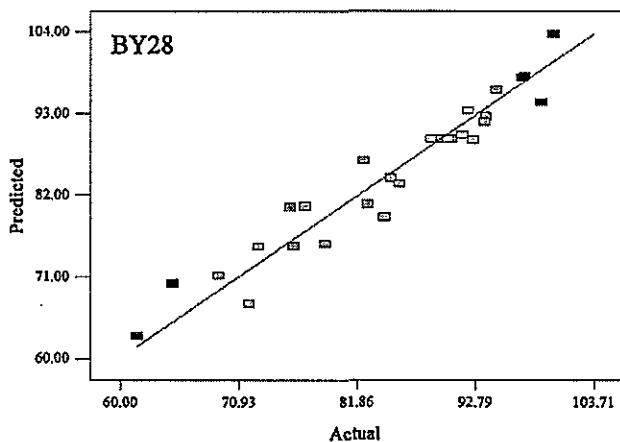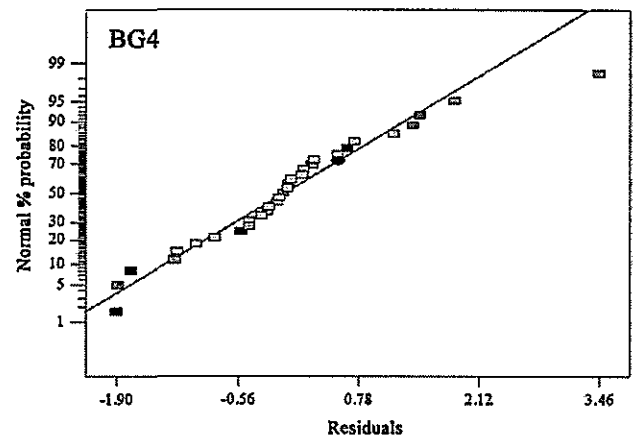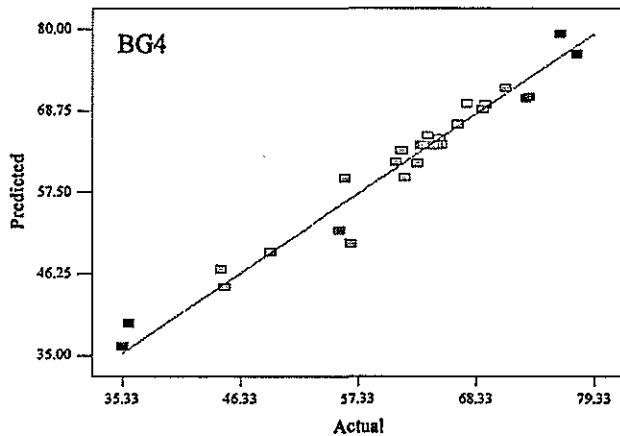

Fig. 5. Comparison of the experimental results of color removal with the predicted values using CCD model.

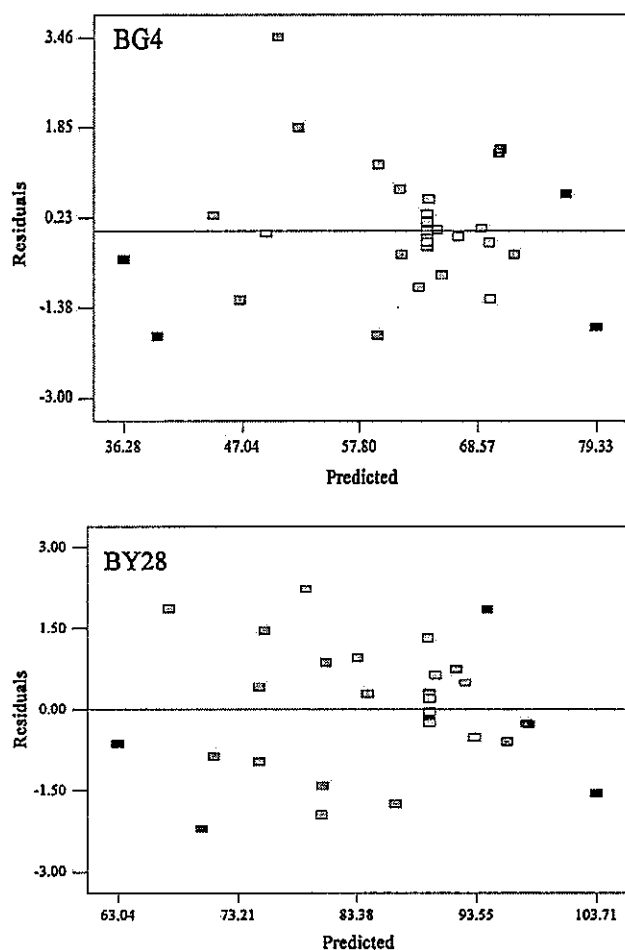**Fig. 6.** Normal probability plots for the removal efficiency of dyes.

Fig. 7. Residual versus predicted response values for the removal efficiency of dyes.

Fig. 8. Pareto graphic analysis of BG4 and BY28.

were so close to the corresponding R^2 values, thereby implying a good correspondence between the predicted and experimental removal efficiency (%). Due to the presence of many terms in the applied model and a sample size not very large, there was a smaller adjusted R^2 [57]. The significance of the model was further probed by the obtained F-value and P-value. Therefore, it can be stated that the larger the quantity of the F-value and the smaller the P-value, the more significant the applied model. The obtained F-value for BG4 and BY28 was calculated to be 28.12 and 14.66, respectively. It was revealed that the obtained F-value for both BG4 and BY28 was much higher than the Fisher's F-value (2.37 at 95% confidence level), thereby indicating the compatibility and adequacy of the model in explaining the adsorption of cationic dyes onto chemically modified nanoclay (Table 4). In addition, the evaluation of the residuals may be considered an appropriate tool to show how well the model satisfies the assumptions of the ANOVA [27,36]. This analysis involves the identification of the outliers and examination of diagnostic plots such as normal probability and residual plots. Normal probability plots show whether or not the residuals follow a normal distribution [58]. The plots of normal probability of the residuals for BG4 and BY28 have been depicted in Fig. 6. As shown, there were reasonably well-behaved residuals in the case of both BG4 and BY28 and the residuals were normally distributed, resembling a straight line. Furthermore, residuals versus predicted responses were plotted as given in Fig. 7. The plot was expected to be a random scatter with a constant range of residuals across the graph. As illustrated in Fig. 7, the residuals in
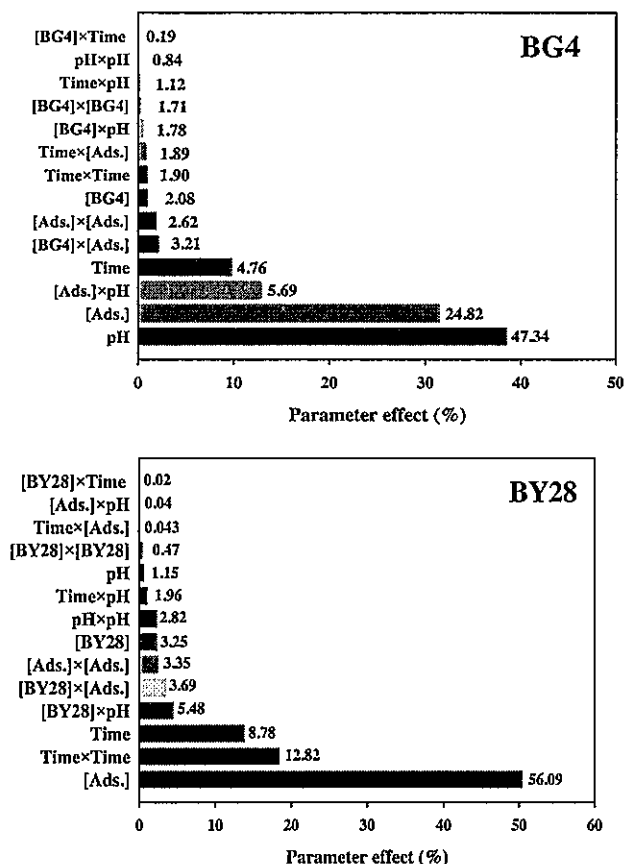
the plot fluctuated in a random pattern around the center line. Besides, the Pareto analysis yielded more significant information that could help to interpret the results of response surface modeling. In fact, this analysis could be used to estimate the percentage effect of each factor on the response (removal efficiency (%)) as shown in Eq. (8) [57]:

$$P_i = \left(\frac{b_i^2}{\sum b_i^2} \right) \times 100 (i \neq 0) \tag{8}$$

The Pareto graphic analysis of BG4 and BY28 can be seen in Fig. 8. As shown, the pH of the solution (47.34%) and the adsorbent dosage (56.09%) exerted the main effect on the adsorption of BG4 and BY28, respectively.

To obtain the best fitted and simpler model for two dyes removal efficiency, insignificant terms with P-values higher 0.05 than can be removed from the CCD model. The final quadratic response surface model is shown in coded form as follows:

$$Y(BG4) = 63.9445 + 3.6488X_2 + 6.5513X_3 + 7.2494X_4$$
$$- 1.6024X_3^2 + 1.7056X_1X_3 - 4.1853X_3X_4 \tag{9}$$

$$Y(BY28) = 89.5526 - 1.6422X_1 + 4.0007X_2 + 7.6507X_3$$
$$- 4.6280X_2^2 - 1.7140X_3^2 + 1.6394X_4^2 - 2.0096X_1X_3$$
$$- 2.2784X_1X_4 \tag{10}$$

Table 5

Estimated coefficients and corresponding F, t and P-values.

Term	Coefficient estimate		Standard error		F-value		Student t		P-value	
	BG4	BY28	BG4	BY28	BG4	BY28	BG4	BY28	BG4	BY28
X_0	63.9445	89.5526	1.0620	1.4083	–	–	60.209	63.590	0.000	0.000
X_1	1.1458	−1.6422	0.5736	0.7606	3.99	4.66	1.998	-2.159	0.063	0.046
X_2	3.6488	4.0007	0.5736	0.7606	40.47	27.67	6.362	5.260	0.000	0.000
X_3	6.5513	7.6507	0.5736	0.7606	130.46	101.19	11.422	10.059	0.000	0.000
X_4	7.2494	0.8237	0.5736	0.7606	159.75	1.17	12.639	1.083	0.000	0.295
X_{11}	−0.5355	−0.6951	0.5255	0.6968	1.04	1.00	−1.019	−0.998	0.323	0.333
X_{22}	−1.1093	−4.6280	0.5255	0.6968	4.46	44.12	−2.111	−6.642	0.051	0.000
X_{33}	−1.6024	−1.7140	0.5255	0.6968	9.30	6.05	−3.050	−2.460	0.008	0.026
X_{44}	0.2215	1.6394	0.5255	0.6968	0.18	5.54	0.422	2.353	0.679	0.032
X_{12}	0.1689	0.0007	0.7025	0.9315	0.06	0.00	0.240	0.001	0.813	0.999
X_{13}	1.7056	−2.0096	0.7025	0.9315	5.90	4.65	2.428	−2.157	0.027	0.047
X_{14}	0.8065	−2.2784	0.7025	0.9315	1.32	5.98	1.148	−2.446	0.268	0.026
X_{23}	−1.0232	0.4508	0.7025	0.9315	2.12	0.23	−1.457	0.484	0.165	0.635
X_{24}	−0.4478	1.0886	0.7025	0.9315	0.41	1.37	−0.638	1.169	0.533	0.260
X_{34}	−4.1853	−0.4197	0.7025	0.9315	35.50	0.20	−5.958	−0.451	0.000	0.658

3.3. Significance of the regression coefficients

The regression coefficient values, standard error, calculated t and F values and significance levels can be seen in Table 5. It could be observed that linear coefficients X_2, X_3 and X_4, quadratic coefficient X_{33} and the interaction coefficient X_{13} and X_{34} for BG4 were all significant at a confidence level of 95%. Therefore, it was inferred that statistically significant parameters represented the linear effect of contact time, adsorbent dosage and the pH of the solution, the quadratic effect of adsorbent dosage and the interaction effect of the adsorbent dosage with pH of the solution and dye concentration with adsorbent dosage. In the case of BY28, the linear effect of the dye concentration, contact time and adsorbent dosage and the quadratic effect of contact time, adsorbent dosage and pH of solution and the interaction effect of dye concentration with the adsorbent dosage and dye concentration with the pH of solution were found to be significant at the same confidence level.

3.4. The effect of variables and their interaction on dye adsorption

To study the influence of four factors simultaneously on the adsorption of dyes, the perturbation plot was employed. The perturbation plot can be used to compare the effect of all factors at a particular point in the design space. Hence, the perturbation plots can show (Fig. 9) the deviation of the factorial level from the adjusted reference point of all variables. To explain more, a steep slope or curvature in a factor indicates that the response can be sensitive to that variable. A relatively flat line, on the other hand, shows response insensitivity to change in that particular variable [37]. As shown in Fig. 9, the initial dye concentration (A), contact time (B), the adsorbent dosage (C) and the pH of the solution (D) were the controlling parameters to obtain the maximum removal efficiency of the dyes. A relatively steep curvature for the pH of the solution indicated that the response of BG4 removal efficiency was sensitive to this parameter. The relatively flat curves for the initial dye concentration showed that the influence of this factor was less on the dye removal, in comparison to the pH of the solution. The contact time curves showed a slow curvature, thereby indicating that this factor had a slight effect on the response. As can be seen in Fig. 9, in the case of BY28, the removal efficiency showed sensitivity to the change in contact time and adsorbent dosage levels. It could be concluded that adsorption of dyes was considerably dependent on its adsorbent dosage for both BG4 and BY28.

Three dimensional (3D) and corresponding contour plots were plotted based on the polynomial function model in order to analyze the interactive effect of the studied operational parameters on the adsorption of BG4 and BY28. The response surface plots (3-D) and corresponding contour plots can be useful in

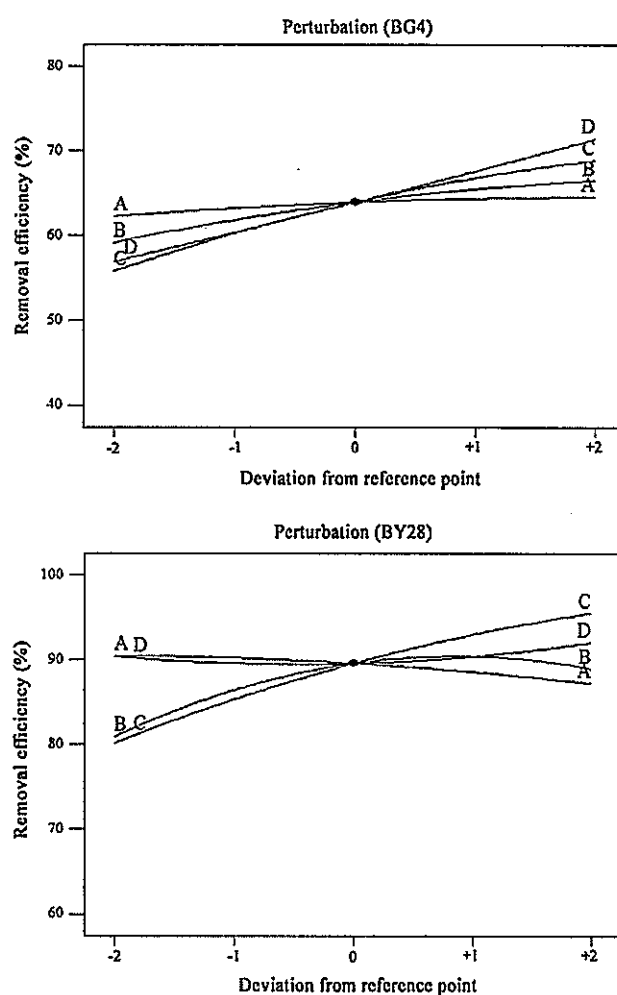**Perturbation (BG4)**

Perturbation (BY28)

Fig. 9. Perturbation plots for the removal of BG4 and BY28 using chemically modified nanoclay. (A) Dye initial concentration; (B) contact time; (C) adsorbent dosage; and (D) pH.
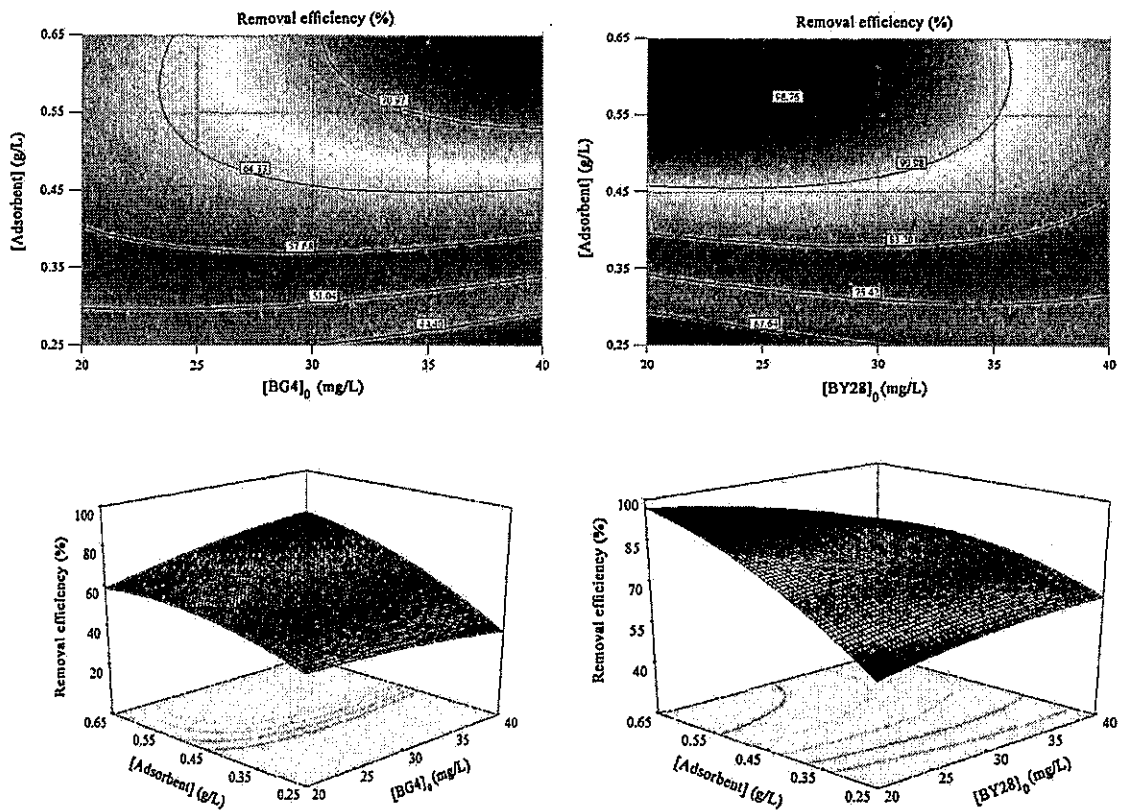
Fig. 10. The response surface and contour plots of the dye removal efficiency (%) as a function of dye initial concentration and adsorbent dosage (contact time = 35 min g/L, and pH 6).
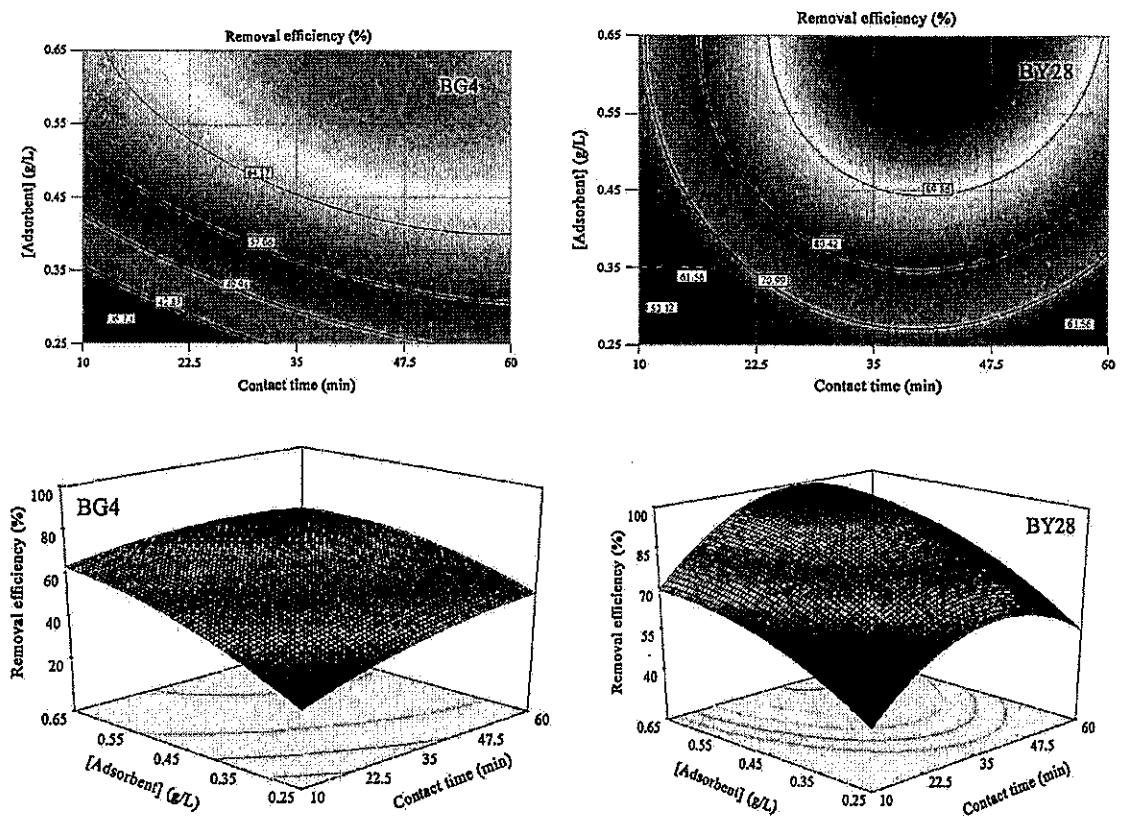

Fig. 11. The response surface and contour plots of the dye removal efficiency (%) as a function of adsorbent dosage and contact time (Dye = 30 mg/L, and pH 6).
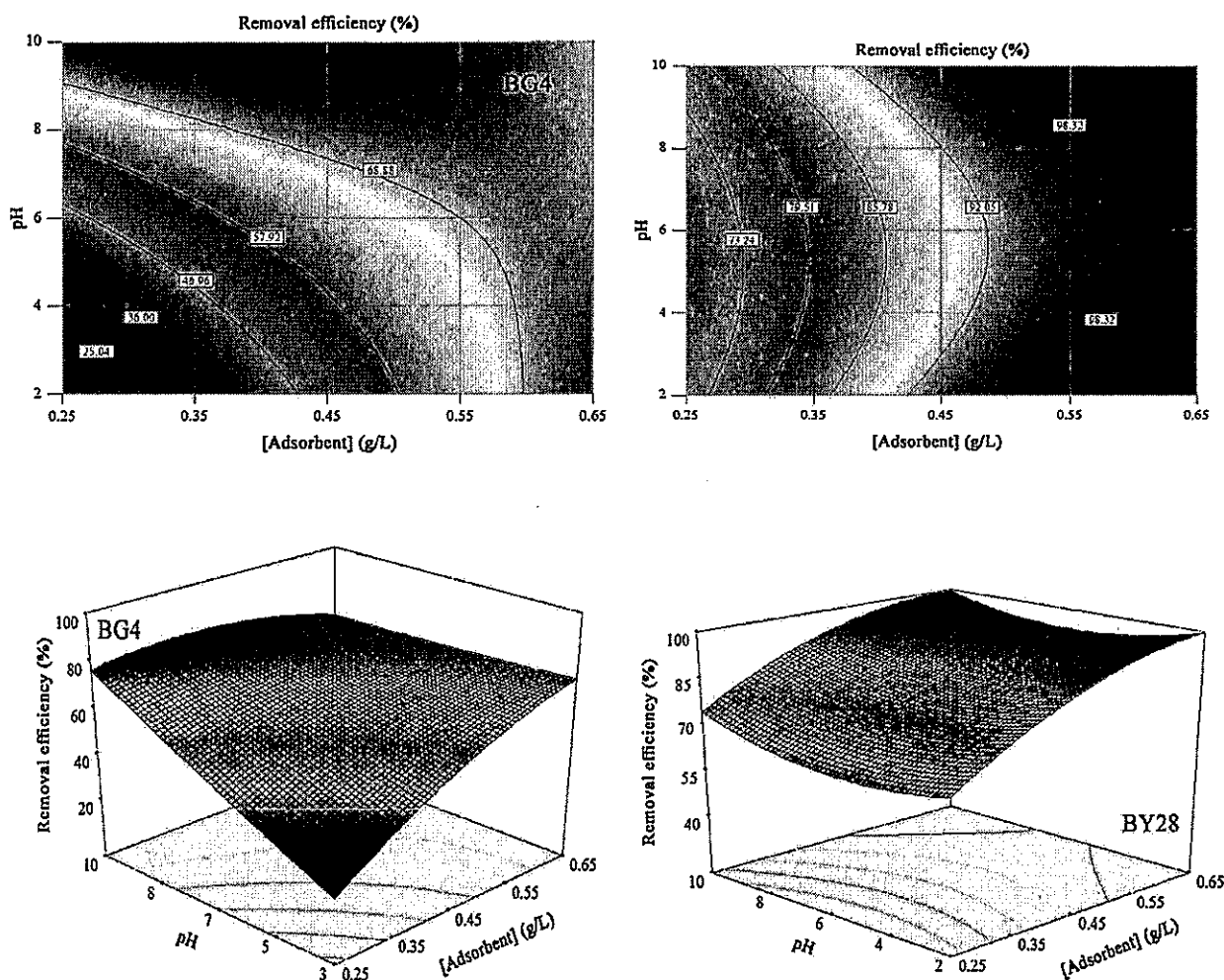
Fig. 12. The response surface and contour plots of the dye removal efficiency (%) as a function of pH and adsorbent dosage (Dye = 30 mg/L, and contact time = 35 min).

understanding the interactive effects of the selected independent variables [27]. Response surface plots can regarded as an approach to predict removal efficiency (%) for different values of the tested variables. Also, contours plots are helpful to distinguish the type of interactions between the studied variables. Fig. 10 shows the response surface and contour plots as a function of the initial dye concentration and adsorbent dosage while the contact time and pH of the solution were kept constant at 35 min and 6, respectively. As can be seen in Fig. 10, the removal efficiency of dye was decreased with increasing the initial dye concentration. Reduction in dye removal efficiency (%) at high dye concentrations could be due to the saturation of adsorptive sites of the adsorbent [27]. Furthermore, the increase in dye removal efficiency (%) with decreasing initial dye concentrations revealed that the adsorption of both BG4 and BY28 was dependent on their initial concentrations. Fig. 10 shows the interactive effect of the initial dye concentration and the adsorbent dosage on the dye removal (%) when the contact time and the pH of the solution were constant at 35 min and 6, respectively. As can be seen, increasing adsorbent dosage resulted in a sharp increase in dye removal (%), thereby indicating that the adsorbent dosage had a major effect on dye removal (%) for both BG4 and BY28. This could be further verified by the obtained F-value of adsorbent dosage (Table 5). Increasing adsorbent dosage provided more surface area, thereby leading to more binding sites for the adsorption of target pollutants onto the modified nanoclay [59]. The interactive effect of adsorbent dosage and contact time on

BG4 and BY28 removal efficiencies at 30 mg/L of dye and the pH of 6 are shown in Fig. 11. As can be seen, a relatively strong increase in adsorbent dosage resulted in the removal efficiency (%) of both dyes. It could be, therefore, deduced that removal efficiencies of both dyes were considerably affected by the interaction between the contact time and the adsorbent dosage. This could be verified by observation that the adsorbent dosage had an appreciable amount of F-value for the adsorbent dosage as compared to other factors (Table 5). In the case of BY28, removal efficiency (%) was significantly affected by the interaction between the contact time and the adsorbent dosage, in comparison to BG4. The response surface and contour plots of the interaction effect of the pH of the solution and adsorbent dosage can be seen in Fig. 12. The removal efficiency (%) of both dyes was increased with an increase in the adsorbent dosage regardless of the high or low value of pH. Increasing the removal efficiency (%) of dyes could be achieved by the simultaneous increase in the adsorbent dosage and the pH of the solution. Unlike adsorbent dosage, the effect of the pH of the solution on the adsorption of dyes was negligible. The effect of adsorbent dosage was higher than that of the initial pH, in which increasing the adsorbent dosage caused a rapid increase in the removal efficiency (%). This was verified by the smaller F-value for the pH of the solution as compared with other parameters (Table 5). The most important factors were the adsorbent surface area and the availability of more active sites [18].

Table 6
Obtained optimum values of the process variables and responses.

Variable	Optimum value	
	BG4	BY28
[Dye]$_0$ (mg/L)	40	20
Contact time (min)	52	60
Adsorbent dosage (g/L)	0.4561	0.4006
pH	10	10
Removal efficiency (%) (pred.)	84.68	95.00
Removal efficiency (%) (exp.)	82.35	98.78

3.5. Process optimization

One of the major objectives of this work was finding the optimum process parameters in order to maximize the removal of dyes using the mathematical model proposed. To this aim, numerical optimization was employed to determine desirable values for each parameter to reach the maximum removal efficiency (%). Table 6 summarizes the results of numerical optimization for the adsorption of both BG4 and BY28 onto chemically modified nanoclay. The results obtained by numerical optimization for BG4 revealed that a maximum removal efficiency (%) of 84.68% could be obtained with the initial BG4 concentration of 40 mg/L, the adsorbent dosage of 0.45 g/L, the contact time of 52 min and the solution pH of 10. In the case of BY28, a maximum removal efficiency (%) of 95.00% was achieved with the initial BY28 concentration of 20 mg/L, the adsorbent dosage of 0.40 g/L, the contact time of 60 min and the solution pH of 10. In order to validate the obtained results, additional experiments were conducted under optimized values in order to verify the results of the numerical optimization. It was found that under optimum operational parameters, the experimental removal efficiency (%) for BG4 and BY28 was 82.35% and 98.78%, respectively. This showed the reliability of the applied model for the appraisal of the real conditions.

3.6. Possible adsorption mechanism

It is known that chemically modified nanoclay particles have a negative surface charge at natural pH (-15.8 mV), owing to the presence of negatively charged functional groups (Si—O and Al—O groups). Various adsorption mechanisms can be proposed in this regard. One of them is the electrostatic interactions between negatively charged functional groups on the modified nanoclay surface and ions that come from the dye molecules. The second one involves hydrogen bonds carrying Si—OH, Al—OH and N—H groups of the adsorbent and oxygen and nitrogen containing groups of the dye molecules. Also, the possibility of hydrophobic interaction between long chain alkyl groups of the modified nanoclay and dye molecules should be considered.

4. Conclusion

Central composite design was used for the optimization of process parameters on the adsorption of two textile dyes onto chemically modified nanoclay. For this purpose, experiments were carried out as a function of initial dye concentration, contact time, adsorbent dosage and the pH of the solution. The results obtained from ANOVA and subsequently, the linear effect of four experimental parameters revealed that CCD model could be regarded as an effective approach for the optimization of the experimental variables. Adsorbent dosage was found to be the most influential parameter. However, the adsorption of BY28 was relatively more efficient and rapid than that of BG4. Additionally, the results of

Pareto analysis indicated that the pH of the solution and the adsorbent dosage had a significant effect on the removal of BG4 and BY28, respectively. Predicted values obtained using the models equations were found to be in a good agreement with the experimental values ($R^2 = 0.960$ for BG4 and $R^2 = 0.927$ for BY28). Therefore, it can be concluded that commercial chemically modified nanoclay is an efficient adsorbent with quite good capability for the removal of BG4 and BY28 dyes from the aqueous phase.

References

[1] E.N. El Qada, S.J. Allen, G.M. Walker, Adsorption of methylene blue onto activated carbon produced from steam activated bituminous coal: a study of equilibrium adsorption isotherm, Chem. Eng. J. 124 (2006) 103–110.
[2] A. Gürses, A. Hassani, M. Kıranşan, Ö. Açışlı, S. Karaca, Removal of methylene blue from aqueous solution using by untreated lignite as potential low-cost adsorbent: kinetic, thermodynamic and equilibrium approach, J. Water Process Eng. 2 (2014) 10–21.
[3] S. Karaca, A. Gürses, Ö. Açışlı, A. Hassani, M. Kıranşan, K. Yıkılmaz, Modeling of adsorption isotherms and kinetics of Remazol Red RB adsorption from aqueous solution by modified clay, Desalin. Water Treat. 51 (2013) 2726–2739.
[4] A. Hassani, R. Darvishi Cheshmeh Soltani, S. Karaca, A. Khataee, Preparation of montmorillonite–alginate nanobiocomposite for adsorption of a textile dye in aqueous phase: Isotherm, kinetic and experimental design approaches, J. Ind. Eng. Chem. 21 (2015) 1197–1207.
[5] A. Khataee, L. Alidokht, A. Hassani, S. Karaca, Response surface analysis of removal of a textile dye by a Turkish coal powder, Adv. Environ. Res. 2 (2013) 291–308.
[6] M.B. Gholivand, Y. Yamini, M. Dayeni, S. Seidi, E. Tahmasebi, Adsorptive removal of alizarin red-S and alizarin yellow GG from aqueous solutions using polypyrrole-coated magnetic nanoparticles, J. Environ. Chem. Eng. 3 (2015) 529–540.
[7] P. Cañizares, F. Martínez, C. Jiménez, J. Lobato, M.A. Rodrigo, Coagulation and electrocoagulation of wastes polluted with dyes, Environ. Sci. Technol. 40 (2006) 6418–6424.
[8] N. Daneshvar, A.R. Khataee, A.R. Amani Ghadim, M.H. Rasoulifard, Decolorization of C.I. Acid Yellow 23 solution by electrocoagulation process: investigation of operational parameters and evaluation of specific electrical energy consumption (SEEC), J. Hazard. Mater. 148 (2007) 566–572.
[9] S. Zinadini, A.A. Zinatizadeh, M. Rahimi, V. Vatanpour, H. Zangeneh, M. Beygzadeh, Novel high flux antifouling nanofiltration membranes for dye removal containing carboxymethyl chitosan coated Fe$_3$O$_4$ nanoparticles, Desalination 349 (2014) 145–154.
[10] N. Modirshahla, A. Hassani, M.A. Behnajady, R. Rahbarfam, Effect of operational parameters on decolorization of Acid Yellow 23 from wastewater by UV irradiation using ZnO and ZnO/SnO$_2$ photocatalysts, Desalination 271 (2011) 187–192.
[11] A.R. Khataee, M. Safarpour, A. Naseri, M. Zarei, Photoelectro-Fenton/nanophotocatalysis decolorization of three textile dyes mixture: response surface modeling and multivariate calibration procedure for simultaneous determination, J. Electroanal. Chem. 672 (2012) 53–62.
[12] J.-H. Sun, S.-P. Sun, G.-L. Wang, L.-P. Qiao, Degradation of azo dye Amido black 10B in aqueous solution by Fenton oxidation process, Dyes Pigm. 74 (2007) 647–652.
[13] N.A. Zubir, C. Yacou, X. Zhang, J.C. Diniz da Costa, Optimisation of graphene oxide-iron oxide nanocomposite in heterogeneous Fenton-like oxidation of Acid Orange 7, J. Environ. Chem. Eng. 2 (2014) 1881–1888.
[14] A.R. Khataee, A. Movafeghi, S. Torbati, S.Y. Salehi Lisar, M. Zarei, Phytoremediation potential of duckweed (Lemna minor L.) in degradation of C.I. Acid Blue 92: artificial neural network modeling, Ecotox. Environ. Safe. 80 (2012) 291–298.
[15] A.R. Khataee, G. Dehghan, M. Zarei, E. Ebadi, M. Pourhassan, Neural network modeling of biotreatment of triphenylmethane dye solution by a green macroalgae, Chem. Eng. Res. Des. 89 (2011) 172–178.
[16] R. Darvishi Cheshmeh Soltani, A.R. Khataee, M. Safari, S.W. Joo, Preparation of bio-silica/chitosan nanocomposite for adsorption of a textile dye in aqueous solutions, Int. Biodeter. Biodegr. 85 (2013) 383–391.
[17] E. Daneshvar, M. Kousha, M.S. Sohrabi, A. Khataee, A. Converti, Biosorption of three acid dyes by the brown macroalga Stoechospermum marginatum: isotherm, kinetic and thermodynamic studies, Chem. Eng. J. 195–196 (2012) 297–306.
[18] M. Kıranşan, R. Darvishi Cheshmeh Soltani, A. Hassani, S. Karaca, A. Khataee, Preparation of cetyltrimethylammonium bromide modified montmorillonite nanomaterial for adsorption of a textile dye, J. Taiwan Inst. Chem. Eng. 45 (2014) 2565–2577.

[19] A. Gürses, Ç. Doğar, S. Karaca, M. Açıkyıldiz, R. Bayrak, Production of granular activated carbon from waste Rosa canina sp. seeds and its adsorption characteristics for dye, J. Hazard. Mater. 131 (2006) 254–259.

[20] N. Gupta, A.K. Kushwaha, M.C. Chattopadhyaya, Adsorption studies of cationic dyes onto Ashoka (*Saraca asoca*) leaf powder, J. Taiwan Inst. Chem. Eng. 43 (2012) 604–613.

[21] R. Darvishi Cheshmeh Soltani, G. Shams Khorramabadi, A.R. Khataee, S. Jorfi, Silica nanopowders/alginate composite for adsorption of lead (II) ions in aqueous solutions, J. Taiwan Inst. Chem. Eng. 45 (2014) 973–980.

[22] G. Shams Khorramabadi, R. Darvishi Cheshmeh Soltani, A. Rezaee, A.R. Khataee, A. Jonidi Jafari, Utilisation of immobilised activated sludge for the biosorption of chromium (VI), Can. J. Chem. Eng. 90 (2012) 1539–1546.

[23] Z. Noorimotlagh, R. Darvishi Cheshmeh Soltani, A.R. Khataee, S. Shahriyar, H. Nourmoradi, Adsorption of a textile dye in aqueous phase using mesoporous activated carbon prepared from Iranian milk vetch, J. Taiwan Inst. Chem. Eng. 45 (2014) 1783–1791.

[24] M. Uğurlu, A. Gürses, M. Açıkyıldız, Comparison of textile dyeing effluent adsorption on commercial activated carbon and activated carbon prepared from olive stone by ZnCl₂ activation, Micropor. Mesopor. Mater. 111 (2008) 228–235.

[25] L. Wang, J. Zhang, R. Zhao, C. Li, Y. Li, C. Zhang, Adsorption of basic dyes on activated carbon prepared from *Polygonum orientale* Linn.: equilibrium, kinetic and thermodynamic studies, Desalination 254 (2010) 68–74.

[26] Y. Park, G.A. Ayoko, R.L. Frost, Application of organoclays for the adsorption of recalcitrant organic molecules from aqueous media, J. Colloid Interface Sci. 354 (2011) 292–305.

[27] R. Darvishi Cheshmeh Soltani, A.R. Khataee, H. Godini, M. Safari, M.J. Ghanadzadeh, M.S. Rajaei, Response surface methodological evaluation of the adsorption of textile dye onto biosilica/alginate nanobiocomposite: thermodynamic, kinetic, and isotherm studies, Desalin. Water Treat. (2014) 1–14.

[28] S. Arellano-Cárdenas, S. López-Cortez, M. Cornejo-Mazón, J.C. Mares-Gutiérrez, Study of malachite green adsorption by organically modified clay using a batch method, Appl. Surf. Sci. 280 (2013) 74–78.

[29] L. Guz, G. Curutchet, R.M. Torres Sánchez, R. Candal, Adsorption of crystal violet on montmorillonite (or iron modified montmorillonite) followed by degradation through Fenton or photo-Fenton type reactions, J. Environ. Chem. Eng. 2 (2014) 2344–2351.

[30] A. Hassani, M. Kıranşan, R. Darvishi Cheshmeh Soltani, A.R. Khataee, S. Karaca, Optimization of the adsorption of a textile dye onto nanoclay using a central composite design, Turk. J. Chem. 39 (2015) 734–749.

[31] P. Yuan, D. Liu, D.-Y. Tan, K.-K. Liu, H.-G. Yu, Y.-H. Zhong, A.-H. Yuan, W.-B. Yu, H.-P. He, Surface silylation of mesoporous/macroporous diatomite (diatomaceous earth) and its function in Cu(II) adsorption: The effects of heating pretreatment, Micropor. Mesopor. Mater. 170 (2013) 9–19.

[32] B. Gao, P. Jiang, F. An, S. Zhao, Z. Ge, Studies on the surface modification of diatomite with polyethyleneimine and trapping effect of the modified diatomite for phenol, Appl. Surf. Sci. 250 (2005) 273–279.

[33] W.-T. Tsai, C.-W. Lai, K.-J. Hsien, Characterization and adsorption properties of diatomaceous earth modified by hydrofluoric acid etching, J. Colloid Interface Sci. 297 (2006) 749–754.

[34] H. Yang, Q. Feng, Characterization of pore-expanded amino-functionalized mesoporous silicas directly synthesized with dimethyldecylamine and its application for decolorization of sulphonated azo dyes, J. Hazard. Mater. 180 (2010) 106–114.

[35] C. L. Zheng, Y. Wang, X. Shu, L. Li Yan, Utilization of diatomite/chitosan-Fe (III) composite for the removal of anionic azo dyes from wastewater: equilibrium, kinetics and thermodynamics, Colloids Surf. A 468 (2015) 129–139.

[36] R. Darvishi Cheshmeh Soltani, A. Rezaee, A.R. Khataee, M. Safari, Photocatalytic process by immobilized carbon black/ZnO nanocomposite for dye removal from aqueous medium: optimization by response surface methodology, J. Ind. Eng. Chem. 20 (2014) 1861–1868.

[37] A. Hassani, L. Alidokht, A.R. Khataee, S. Karaca, Optimization of comparative removal of two structurally different basic dyes using coal as a low-cost and available adsorbent, J. Taiwan Inst. Chem. Eng. 45 (2014) 1597–1607.

[38] A.R. Khataee, M. Zarei, M. Fathinia, M.K. Jafari, Photocatalytic degradation of an anthraquinone dye on immobilized TiO₂ nanoparticles in a rectangular re-

actor: destruction pathway and response surface approach, Desalination 268 (2011) 126–133.

[39] J.P. Silva, S. Sousa, I. Gonçalves, J.J. Porter, S. Ferreira-Dias, Modelling adsorption of acid orange 7 dye in aqueous solutions to spent brewery grains, Sep. Purif. Technol. 40 (2004) 163–170.

[40] F. Rasouli, S. Aber, D. Salari, A.R. Khataee, Optimized removal of Reactive Navy Blue SP-BR by organo-montmorillonite based adsorbents through central composite design, Appl. Clay Sci. 87 (2014) 228–234.

[41] R.-L. Tseng, S.-K. Tseng, Characterization and use of high surface area activated carbons prepared from cane pith for liquid-phase adsorption, J. Hazard. Mater. 136 (2006) 671–680.

[42] A.R. Khataee, M.B. Kasiri, L. Alidokht, Application of response surface methodology in the optimization of photocatalytic removal of environmental pollutants using nanocatalysts, Environ. Technol. 32 (2011) 1669–1684.

[43] J. Liu, M. Dong, S. Zuo, Y. Yu, Solvothermal preparation of TiO₂/montmorillonite and photocatalytic activity, Appl. Clay Sci. 43 (2009) 156–159.

[44] S. Miao, Z. Liu, B. Han, J. Zhang, X. Yu, J. Du, Z. Sun, Synthesis and characterization of TiO₂-montmorillonite nanocomposites and their application for removal of methylene blue, J. Mater. Chem. 16 (2006) 579–584.

[45] M.J. Rosen, Surfactants and Interfacial Phenomena, John Wiley & Sons, New York, 1978.

[46] S.J. Gregg, K.S.W. Sing, Adsorption, Surface Area and Porosity, 2nd ed., Academic Press, London, 1982.

[47] W.-T. Tsai, J.-M. Yang, H.-C. Hsu, C.-M. Lin, K.-Y. Lin, C.-H. Chiu, Development and characterization of mesoporosity in eggshell ground by planetary ball milling, Micropor. Mesopor. Mater. 111 (2008) 379–386.

[48] F. Adam, J.N. Appaturi, R. Thankappan, M.A.M. Nawi, Silica–tin nanotubes prepared from rice husk ash by sol-gel method: characterization and its photocatalytic activity, Appl. Surf. Sci. 257 (2010) 811–816.

[49] N. Passe-Coutrin, S. Altenor, D. Cossement, C. Jean-Marius, S. Gaspard, Comparison of parameters calculated from the BET and Freundlich isotherms obtained by nitrogen adsorption on activated carbons: a new method for calculating the specific surface area, Micropor. Mesopor. Mater. 111 (2008) 517–522.

[50] R.-S. Juang, F.-C. Wu, R.-L. Tseng, Characterization and use of activated carbons prepared from bagasses for liquid-phase adsorption, Colloids Surf. A. 201 (2002) 191–199.

[51] A.C. Suwandi, N. Indraswati, S. Ismadji, Adsorption of N-methylated diaminotriphenilmethane dye (malachite green) on natural rarasaponin modified kaolin, Desalin. Water Treat. 41 (2012) 342–355.

[52] Y. Ma, J. Zhu, H. He, P. Yuan, W. Shen, D. Liu, Infrared investigation of organo-montmorillonites prepared from different surfactants, Spectrochim. Acta A 76 (2010) 122–129.

[53] W. Xue, H. He, J. Zhu, P. Yuan, FTIR investigation of CTAB–Al–montmorillonite complexes, Spectrochim. Acta A 67 (2007) 1030–1036.

[54] M.H. Baki, F. Shemirani, R. Khani, M. Bayat, Applicability of diclofenac-montmorillonite as a selective sorbent for adsorption of palladium(II): kinetic and thermodynamic studies, Anal. Methods 6 (2014) 1875–1883.

[55] M. Fathinia, A.R. Khataee, M. Zarei, S. Aber, Comparative photocatalytic degradation of two dyes on immobilized TiO₂ nanoparticles: effect of dye molecular structure and response surface approach, J. Mol. Catal. A: Chem. 333 (2010) 73–84.

[56] K.P. Singh, S. Gupta, A.K. Singh, S. Sinha, Optimizing adsorption of crystal violet dye from water by magnetic nanocomposite using response surface modeling approach, J. Hazard. Mater. 186 (2011) 1462–1473.

[57] A.R. Khataee, M. Zarei, L. Moradkhannejhad, Application of response surface methodology for optimization of azo dye removal by oxalate catalyzed photoelectro-Fenton process using carbon nanotube-PTFE cathode, Desalination 258 (2010) 112–119.

[58] L. Alidokht, A.R. Khataee, A. Reyhanitabar, S. Oustan, Cr(VI) immobilization process in a Cr-spiked soil by zerovalent iron nanoparticles: optimization using response surface methodology, CLEAN-Soil Air Water 39 (2011) 633–640.

[59] M. Kousha, E. Daneshvar, M.S. Sohrabi, N. Koutahzadeh, A.R. Khataee, Optimization of C.I. Acid black 1 biosorption by *Cystoseira indica* and *Gracilaria persica* biomasses from aqueous solutions, Int. Biodeter. Biodegr. 67 (2012) 56–63.